BULLETIN OF THE POLISH ACADEMY OF SCIENCES
TECHNICAL SCIENCES
Vol. 54, No. 4, 2006

Crack system evaluation in concrete elements at mesoscale

M.A. GLINICKI* and A. LITOROWICZ

Institute of Fundamental Technological Research, Polish Academy of Sciences, 21 Świętokrzyska St., 00-049 Warszawa, Poland

Abstract. An automated method for crack identification and quantitative description of crack systems in concrete was developed in order to aid a service life assessment of concrete elements in structures. Flat polished specimens for crack analysis were impregnated with epoxy resin containing fluorescent dye. The examination of the crack system was performed in ultraviolet light using a stereomicroscope and an Image Pro Plus image analysis system on specimens cored out of several concrete structures. The laboratory tests were performed on cast specimens to establish correlations between water penetration and chloride diffusion and crack system parameters. The analysis of cracks in concrete cores taken from structures resulted in interesting conclusions based on the crack width distribution and crack localization with respect to steel reinforcement. The method was found very effective to support standard concrete diagnostics methods.

Key words: cracks, crack pattern, image analysis, concrete structures.

1. Introduction

The presence of cracks is a characteristic structural feature of most cement-based materials. Microcracking may take place first as a consequence of the partial segregation of the aggregates and plastic shrinkage while the fresh concrete is setting. Temperature differences and drying shrinkage promote further cracking of concrete. After the concrete hardens, various factors aggravate the already existing microcracks and cause the initiation of new ones. It is thought that cracks, whatever their origin is (mechanical, thermal, chemical etc.), can act as major pathways for water or aggressive chemical ions to penetrate into concrete, enabling its deterioration [1,2].

The different damage acquired and the conditions of crack propagation influence the post-damage behaviour and quality of concrete in the cover layer. Durability of concrete structures and the corrosion of reinforcing steel are intimately linked to the water permeability of exposed concrete surfaces, such as pavements, parking slabs and bridge decks. Quantitative investigation of the crack system in concrete can thus provide substantial insight into the deterioration and failure processes of the concrete-based infrastructure.

Several techniques have been developed over the past 4 decades to detect and measure cracks in cement-based materials. These include acoustic emission [3], microscopy techniques [4,5], x-ray techniques [6], etc. Recent developments in microscopy and image processing techniques have facilitated efforts towards investigation of the crack system in concrete [7,8]. Due to the heterogeneity and complexity of the concrete structure a definition of the crack system should be related to the level of observation (resolution of the testing method) as schematically shown in Fig.1.

Automation of image processing and analysis procedures can facilitate practical use of image analysis in identification and quantification of cracks in concrete towards the development of valuable crack structure-property relationships. The prerequisite for the application of image processing and analysis techniques to concrete microscopic images is a proper preparation of specimens so that the features of interest (cracks) develop a distinct contrast against the body of concrete. Specimen preparation methods depend generally on the type of microscopy used. Removal of noise and distinction of cracks from other features are also important. In this paper a special application of automatic image analysis for evaluation of crack systems at the meso-level in concrete elements is presented. To evaluate the suitability of such a test method for concrete quality determination an experimental investigation was performed using concrete specimens made in the laboratory. Moreover, the crack system in some concrete elements sawn out of existing concrete structures damaged by various mechanisms was also quantitatively evaluated.

2. Method for identification and quantification of crack system

2.1. Specimens preparation. A vacuum-impregnated reground plane section technique [10] was used for specimen preparation. Concrete plane sections of thickness of 20–25 mm were obtained by sawing 150-mm cubes (cast) or 100 mm cylinders (cored). The examined surfaces of the specimens were ground, polished and cleaned. Specimens dried in an oven at a temperature of 35°C for 24 h and subsequently at a constant pressure of -1 bar in a vacuum chamber were filled with the epoxy resin containing fluorescent dye. The final curing in an oven was performed at the temperature of 35°C for 24 h. The epoxy penetrated into the specimen and hardened in cracks and other defects. An excess of resin at the surface of the specimen was removed by grinding down 2 mm from the surface.

Microscopic observation of the impregnated reground polished specimens was performed by means of an optical microscope at a magnification of $10\times$ in ultraviolet light. The images

*e-mail: mglinic@ippt.gov.pl

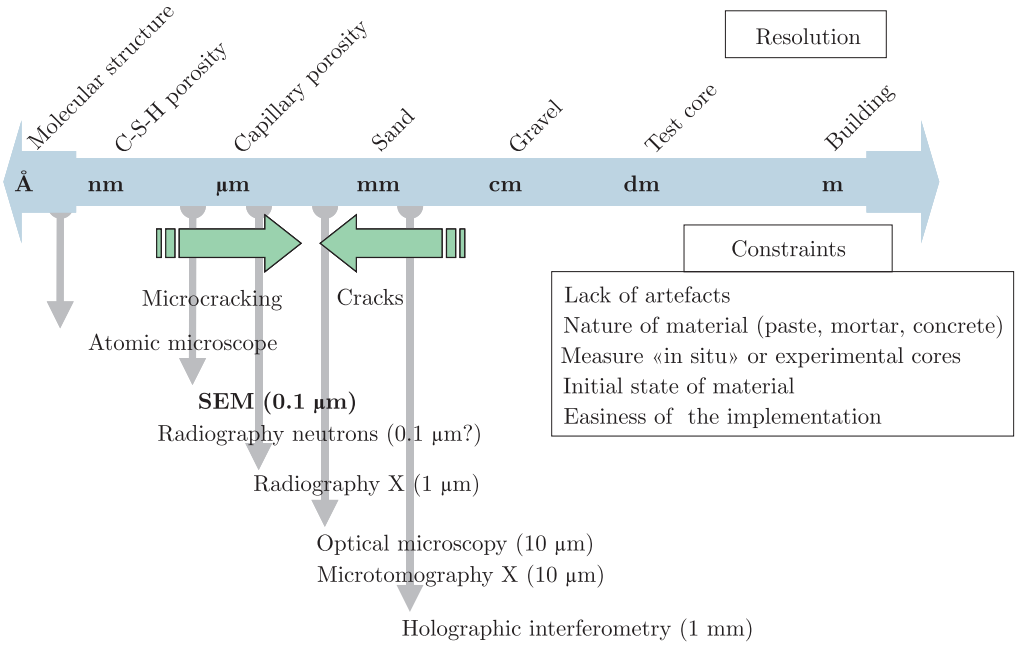

Fig. 1. The resolution of various methods for observation of structure of concrete (after Ref. 9)

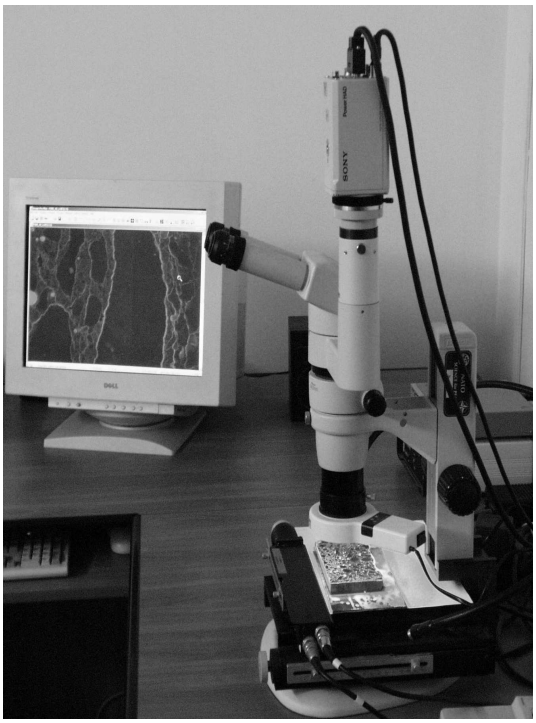

Fig. 2. The test set-up for digital analysis of concrete flat sections

reported in this study were acquired by a video camera (Sony DXC-950P) attached to a Nikon microscope (Fig. 2). Identification of cracks in impregnated specimens was carried out by digital analysis of images using the Image Pro Plus analysis system. The image size acquired on a specimen surface was 25 mm by 61 mm, 25 mm by 52 mm and 32 mm by 52 mm at a magnification of 10. Application of a high precision scanning table allowed capturing of single frames and gluing them together into one image (Fig. 3).

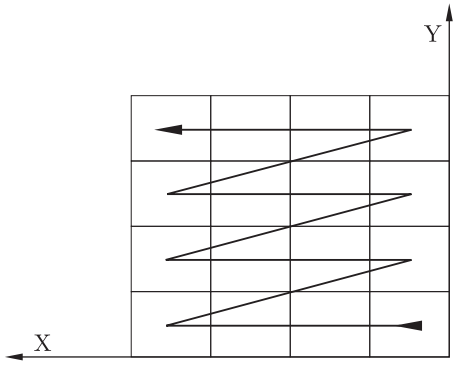

Fig. 3. Movement of the scanning table during image acquisition

To identify the crack network on the specimen surface, the acquired colour image was converted into a binary image on the basis of its R (red), G (green) and B (blue) components by means of a segmentation process. The threshold level for crack identification (the brightest phase in the image – fluorescent resin) in this case was set between: R:0-255, G:120-255, B:0-255. After filtering operations on the binary image and classification of objects according to shape criteria as described in [5], some non-crack objects were removed and cracks were distinguished from other features. The final step of image processing was a reduction of crack thickness to single pixel lines by binary thinning using a filter known as skeletonization.

For identification of cracks on polished sections and description of crack position the following parameters were applied:

– Angle – reports the angle between the vertical axis and the major axis of the ellipse equivalent to the object.
– Area – reports the area of each object.
– Dendritic length – reports the total length of all the dendrites (one-pixel-thick branches).
– PerArea – reports the ratio between the area of the counted object to the entire area of the active image.
– Radius Ratio – reports the ratio between Max Radius and Min Radius for each object; the applied criterion of minimal elongation was: RR > 3.
– Roundness – reports the roundness of each object, as determined by the following formula: perimeter ^{2}/ 4*Π*area; the roundness factor was: Ro > 2.

For description of the crack pattern in concrete specimens the following parameters were used:

– Dendritic length of cracks – L [mm] – total length of all the dendrites of each crack on the image.
– Average width of cracks – W [mm] – total crack area per total dendritic length.
– Area of cracks – A [mm^2] – total area of each crack on the image.
– Density of cracks – L_A [mm/mm^2] – total dendritic length of cracks per image area.
– Areal fraction – A_A [mm^2/mm^2] – ratio between the area of the counted cracks to the entire area of the active image.
– Degree of crack orientation – can be shown by means of "rose of intercepts".
– Distribution of crack width – shown on graph as percentage object fraction in the given range of crack width.

Degree of crack orientation was determined using a classical stereological method of the oriented secants on a plane. The automatic procedure developed for estimation of crack pattern orientation included logical binary operations between two images: image of crack network in concrete and image of parallel equidistant lines (Fig. 4a). The number of intersections $N_L(\Theta)$ of the cracks for a total length of lines L (the specific number of intersections) for a given direction from 0° to 180° by 15° steps was obtained. The degree of orientation was computed according to following equation:

$$\omega = \frac{(N_{Lmax} - N_{Lmin})}{N_{Lmax} + \left(\frac{\Pi}{2} - 1\right) \cdot N_{Lmin}}, \qquad 0 \le \omega \le 1$$

where:
ω – degree of orientation,
N_{Lmax} – maximum values taken by $N_L(\Theta)$ when (Θ) varies,
N_{Lmin} – minimum values taken by $N_L(\Theta)$ when (Θ) varies.

Crack width distribution was estimated by means of an automatic procedure [11]. Cracks on the binary image were subjected to a sorting operation so that they were aligned vertically. Then a logical operation was applied between the image with sorted cracks and the image of parallel equidistant lines perpendicular to the cracks and an image of intersections of cracks with lines was obtained (Fig. 4b). Intersections represented line segments whose length corresponded to the crack width. The results were presented as a percentage object fraction in the given range of crack widths.

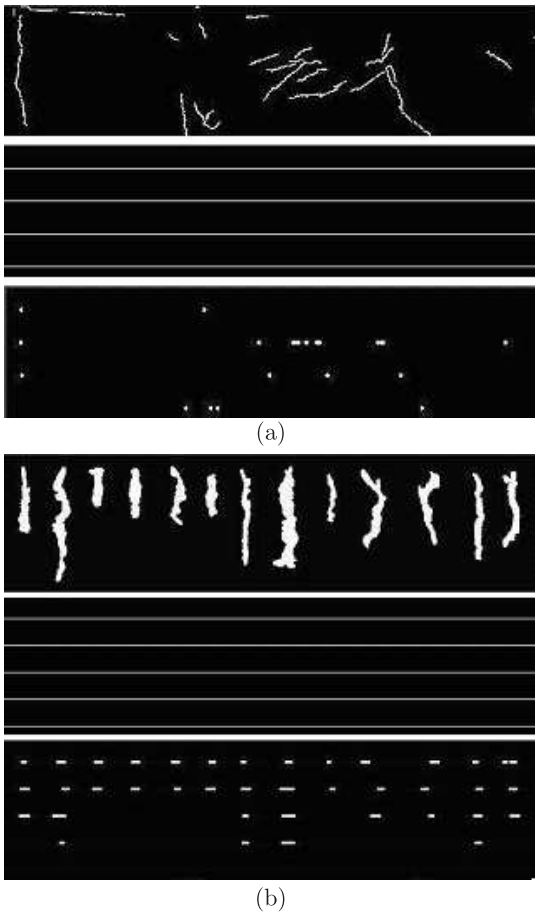

Fig. 4. Illustration of automated procedures: (a) determination of degree of crack orientation, (b) determination of crack width distribution

3. Experiments on laboratory-cast concrete elements

3.1. Materials and specimens. Concrete specimens were manufactured in the laboratory using three Polish cements from Górażdże cement plant: CEM I 32.5 R (Portland cement), CEM II/B-V 32.5 R – HSR (with fly ash) and CEM III/A 32.5 NA (with slag). Crushed basalt and ordinary river sand were used as aggregates. Concrete mixes were designed with constant water to cement ratio of 0.54 (Tabl. 1).

Table 1.
Composition of the concrete mixes

Materials \ Mix designation	CEM I	CEM II	CEM III
	Content [kg/m^3]		
Cement CEM I 32,5R	331		
Cement CEM II/B-V 32,5R		332	
Cement CEM III/A 32,5NA			331
Sand 0–2mm	723	725	723
Crushed basalt 2-8 mm	623	624	622
Crushed basalt 8–16 mm	663	664	662
Water	179	180	179

Concrete mixes were produced in a laboratory mixer; the workability and density of the mix was measured using standard procedures. The concrete was cast in $100 \times 100 \times 100$ mm cubic moulds for compression tests and in $150 \times 150 \times 150$ mm cubic moulds for water penetration tests, chloride migration tests and analysis of crack patterns.

In order to induce cracks, concrete mixes were exposed to freezing action immediately after mixing and after 1 and 2 hours since mixing: the cubes were kept in the climatic chamber at the constant temperature of –5°C. After 2 days of freezing the specimens were demoulded and stored until the age of 28 days in high humidity conditions (RH > 90%) and at a temperature of 20°C. The reference specimens (not subjected to freezing action) were demoulded after 24 hours and then stored in the same conditions.

3.2. Test methods. Manufactured concrete specimens (both cracked and reference ones) were subjected to the following tests: water penetration test, chloride migration test and axial compression test. Some specimens were also cut to make vacuum-impregnated reground plane sections for identification and quantification of crack systems using the method described above.

The water penetration test was performed according to the Polish Standard PN-88/B-06250 on 150 mm cubes. The initial water pressure of 0.2 MPa was applied and maintained for 24 hours. Then the pressure was increased by 0.2 MPa every 24 hours up to 0.8 MPa. After perpendicular splitting of the specimen to the water exposed surface the maximum depth of water penetration was measured. As a result the mean value from measurements on 3 specimens for each series was considered.

The chloride migration coefficient determined according to [12] (a standard method according to Nordtest Method NT BUILD 492) is a measure of the resistance of the tested material to chloride penetration. A cylindrical specimen was drilled out of the half of a 150-mm cube and then a 50 $\pm$2 mm thick disc was sawn. The concrete disc (1 for each series) was placed between two solutions: one end of the disc was in contact with an anolyte (0.3 M NaOH solution) and the other was in contact with a catholyte (10% NaCl solution). A potential was established between an anode immersed in the anolyte and a cathode immersed in the catholyte. The potential was typically 30 V, and it was applied for approximately 24 hours. After exposure, the concrete disc was split longitudinally and the depth to which chloride had penetrated into the sample was determined by the application of silver nitrate solution on the freshly split section, which painted the areas containing chloride ions in white.

The compressive strength of four series of each concrete (reference, frozen immediately and 1 and 2 hours after mixing) was determined on $100 \times 100 \times 100$ mm cubes according to the Polish Standard PN-88/B-06250 (3 for each series).

3.3. Results of laboratory tests. Compressive strength. Table 2 presents the 28-day compressive strengths data. The strength is given as an average value f_c of 3 measurements in each series. As expected, the concrete made with Portland cement CEM I produced the highest strength after 28 days in comparison with concretes CEM II (blended cement with fly ash) and CEM III (blended cement with slag). For the series of concrete CEM I exposed to freezing action after mixing, the compressive strength was significantly reduced – down to 56%, 61% and 65% of reference (undamaged) concrete specimens, respectively for CEM Im0, CEM Im1 and CEM Im2. Concrete CEM II revealed a compressive strength reduction after low-temperature deterioration to about 62%, 75% and 76% of undamaged concrete specimens for CEM IIm0, CEM IIm1 and CEMIIm2, respectively. A similar tendency of compressive strength reduction of concrete subjected to freezing action was shown by concrete CEM III: about 28% strength reduction for concrete CEM IIIm0, 15% – for concrete CEM IIIm1 and 12% – for concrete CEM IIIm2. Strength of concretes exposed to –5°C showed decreasing reduction of compressive strength with retardation of initial freezing age of concrete mixes.

Water penetration test. Depth of water penetration under pressure was determined on specimens after low-temperature deterioration and on reference specimens (Tabl. 2). It can be observed that the water penetration depth for undamaged concrete CEM II was the smallest, 21 mm. For concretes CEM I and CEM III, depth of water penetration was about 2 times larger. Low-temperature damage significantly decreased the resistance to water penetration under pressure: the largest penetration depth was obtained for CEM IIm0, while the smallest was for CEM IIIm2. Only concrete CEM IIm0 was not resistant to water permeability (the water leakage through the specimens was observed). In low-temperature deteriorated concretes the resistance to water penetration increased with retardation of initial freezing age of concrete mixes.

Table 2
Results of compressive strength of concrete and depth of water penetration

Concrete mix			Mean value of compressive strength f_{c28} [MPa]	Mean value of water penetration depth [mm]
CEM I	ref	CEM I	45.81	38
	0	CEM Im0	25.74	140
	1h	CEM Im1	27.99	133
	2h	CEM Im2	29.91	123
CEM II	ref	CEM II	35.19	21
	0	CEM IIm0	22.02	150
	1h	CEM IIm1	26.49	144
	2h	CEM IIm2	26.94	124
CEM III	ref	CEM III	41.70	39
	0	CEM IIIm0	30.15	88
	1h	CEM IIIm1	35.79	52
	2h	CEM IIIm2	36.72	48

ref – reference (undamaged) concrete

m0 – concrete frozen after mixing

m1 – concrete frozen after 1h after mixing

m2 – concrete frozen after 2h after mixing

Chloride migration test. It can be seen in Tab. 3 that reference concrete CEM I (Portland cement) showed higher chloride penetration than reference concretes CEM II (cement with

fly ash) and CEM III (cement with slag), which agrees with other results in the literature [13,14]. Concrete containing mineral additions exhibited higher resistance to chloride ion penetration than concrete with plain Portland cement.

Chloride penetration depths and chloride migration coefficients of the reference concretes were lower in comparison with concretes subjected to freezing action. Differences in the migration coefficient values between reference and damaged concretes are larger for CEM I than for CEM II and CEM III. Concretes subjected to freezing action showed decreased depth of chloride penetration with retardation of initial freezing age of concrete mixes.

Table 3
Results of chloride migration coefficient

Concrete mix			Chloride penetration depth [mm]	Migration coefficient [$\times 10^{-12}$ m^2/s]
CEM I	ref	CEM I	23.71	6.05
	0	CEM Im0	53.71	14.20
	1h	CEM Im1	39.00	12.23
	2h	CEM Im2	37.14	9.88
CEM II	ref	CEM II	13.00	3.21
	0	CEM IIm0	21.14	5.47
	1h	CEM IIm1	18.29	5.57
	2h	CEM IIm2	16.14	4.83
CEM III	ref	CEM III	13.29	3.28
	0	CEM IIIm0	19.43	5.97
	1h	CEM IIIm1	14.86	4.45
	2h	CEM IIIm2	13.71	4.05

Analysis of crack pattern. The cracks were observed in the low-temperature deteriorated concretes only. Table 4 gives the crack characteristics of samples sawn from 150 mm cubes subjected previously to the water penetration test. The deteriorated series of concrete CEM II showed the highest cracks density, while the lowest cracks density was found in series of concrete CEM III. In the analysed concretes, average width of cracks was similar, in the range from 0.075 mm to 0.082 mm. The degree of orientation revealed that cracks were randomly oriented and there was not a definite orientation in the crack pattern. As it is seen from Tabl. 4, the sooner the beginning of freezing of the concrete after mixing, the higher the density of cracks.

Distribution of crack width. Distribution of crack widths is presented in Figs. 5, 6 and 7 as average values of measurements performed on 3 samples in each deteriorated series of concretes CEM I, CEM II and CEM III. For concretes CEM I and CEM II, the distribution of crack widths is similar. Most of the objects are included in the range of crack widths from 0.025 mm to 0.100 mm. In concrete CEM III, the distribution of crack widths moved slightly towards smaller widths. More objects are included in the range of crack widths to 0.025 mm, and less in the range from 0.100 mm to 0.125 mm in comparison with concretes CEM I and CEM II.

As it is seen from Fig. 8, a clear relationship between the compressive strength and density of cracks was found. The compressive strength of concrete decreased with an increase of crack density for each analyzed concrete.

The predominant effect of crack density on depth of water penetration is distinct for the analyzed concretes, especially for CEM I and CEM II. Concrete CEM III showed higher resistance to water penetration than concretes CEM I and CEM II. It is related to a structure of cement paste. Generally concretes with slag exhibit low permeability because of significant decrease of capillary porosity with time of hardening. Also the interfacial zone between the particles of coarse aggregate and the hydrated cement paste is more compacted than in concrete with plain Portland cement. In spite of using different types of cement, the test data fit into one curve (Fig. 9). As can be seen, there is a good correlation between the depth of water penetration and the density of cracks. A correlation between the depth of water penetration and the degree of orientation or width of crack was not observed. From Refs. [2,14] it was noted that in the range of small cracks, up to about 0.1 mm, cracking had a little effect on concrete permeability.

Figure 10 shows the correlation between the depth of chloride penetration and the density of cracks. As was expected, the chloride penetration increased with an increase of crack density. But a relationship between the depth of chloride penetration and the degree of orientation or width of cracks was not noticed. It appears that in the examined heavily deteriorated (cracked) concretes the resistance to water and chloride ion penetration significantly depends on the density of cracks.

Table 4
Results of crack pattern analysis

Concrete mix			Total length [mm]	Area [mm^2]	Average width [mm]	Density [mm/mm^2]	Degree of orientation
CEM I	0	CEM Im0	494.7	38.8	0.078	0.30	0.17
	1h	CEM Im1	449.0	35.5	0.079	0.27	0.19
	2h	CEM Im2	386.6	30.7	0.080	0.23	0.16
CEM II	0	CEM IIm0	681.1	55.5	0.081	0.41	0.24
	1h	CEM IIm1	542.6	40.6	0.075	0.33	0.25
	2h	CEM IIm2	411.4	33.0	0.082	0.25	0.20
CEM III	0	CEM IIIm0	283.3	22.5	0.079	0.17	0.18
	1h	CEM IIIm1	258.0	20.0	0.077	0.16	0.16
	2h	CEM IIIm2	233.0	18.6	0.079	0.14	0.17

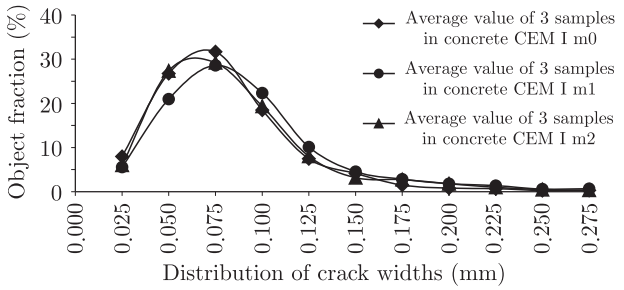

Fig. 5. Distribution of crack widths in samples of concrete CEM I exposed to frost action before hardening

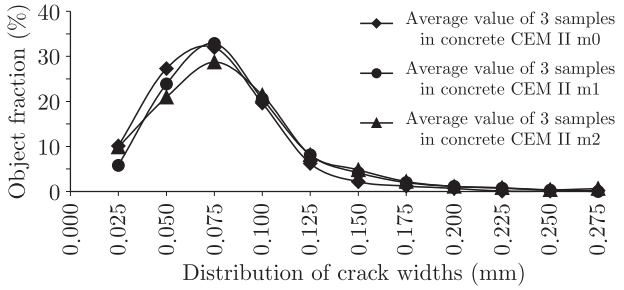

Fig. 6. Distribution of crack widths in samples of concrete CEM II exposed to frost action before hardening

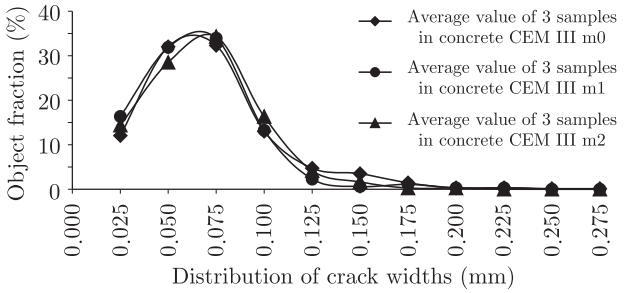

Fig. 7. Distribution of crack widths in samples of concrete CEM III exposed to frost action before hardening

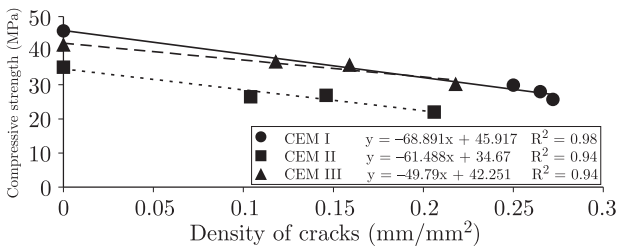

Fig. 8. The relationship between the crack density and the compressive strength of concrete samples exposed to frost action before hardening

4. Application of crack analysis for diagnostics of structures

4.1. Concrete in industrial floor. The developed method for crack identification and quantification of crack systems was applied for the diagnostics of concrete quality at several building sites. In each case such a new diagnostic method was applied along with standard diagnostic methods such as compressive strength tests on concrete cores taken out of structures or nondestructive evaluation of strength using a Schmidt hammer [15]. The microscopic crack analysis on plane sections of specimens prepared from concrete cylinders (diameter of 100 mm) extracted from the industrial floor was performed to evaluate cracking damage. Analysis of crack pattern was performed on images (25×61 mm) acquired in two areas of IRPS (Fig. 11).

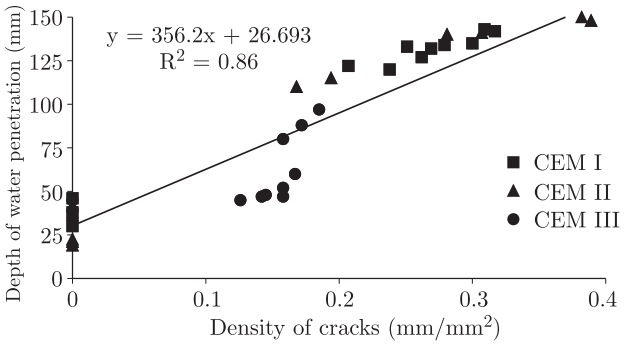

Fig. 9. The relationship between the crack density and the depth of water penetration in concrete

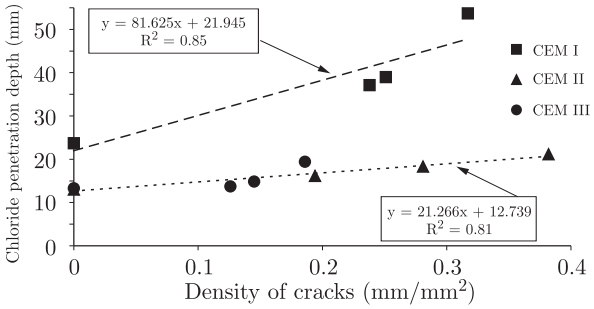

Fig. 10. The relationship between the crack density and the depth of chloride penetration in concrete

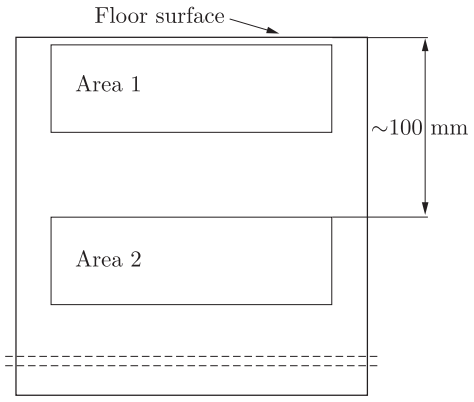

Fig. 11. Two areas of cracks observation

Results of crack density show differences in crack patterns close to the floor surface and at the mid-depth of the slab (Fig. 12). Crack density is several times higher in the surface area and is contained in the range of 0.102–0.170 mm/mm^2, while

in the internal area it is 0.026–0.060 mm/mm^2, if specimen 7 is neglected. In the case of specimen 7, the value of crack density is too high in the internal area because of numerous high porosity areas, which were recognized as cracks by the image analysis system.

According to results of the crack width distribution, the width of most cracks reaches the value 0.1 mm for all specimens (Fig. 13). The average width of cracks is contained in range of 0.06–0.10 mm for all tested specimens.

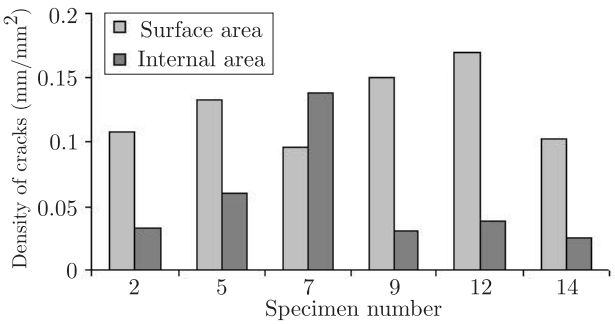

Fig. 12. Density of cracks in concrete samples taken from an industrial floor

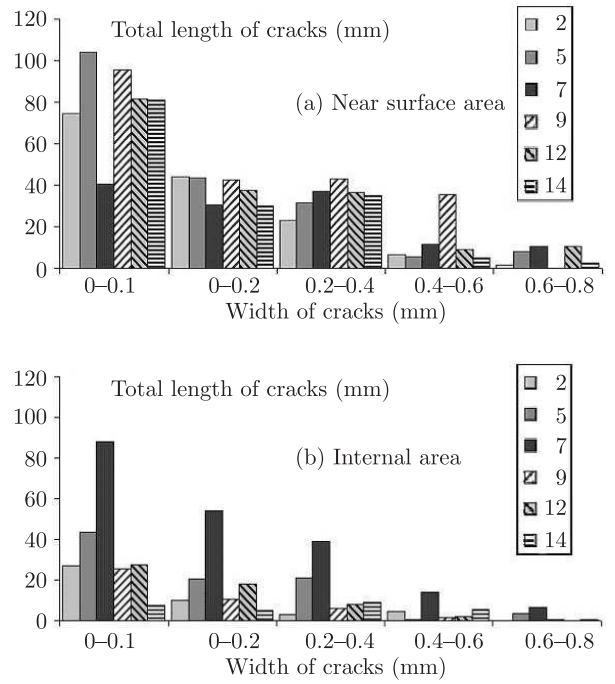

Fig. 13. Distribution of total cracks length in defined ranges of crack width

4.2. Concrete in multistorey parking structure. A diagnostic of the crack system in a multistorey parking structure was performed to estimate probable concrete damage caused due to low-temperature action. The concrete specimens (cylinders with a diameter of 100 mm) were cored out of a slab that was cast in freezing conditions.

Quantitative crack analysis was carried out on images acquired along the specimen height (Fig. 14). It was found that crack density depends on the distance from the exposed surface. The top part of the concrete element was deteriorated by low-temperature action during hardening and the bottom part probably by mechanical action during the structure demolition.

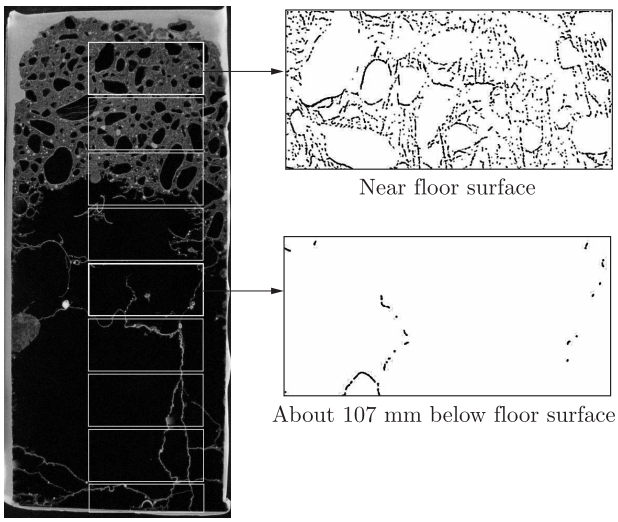

Fig. 14. Example of IRPS (specimen 31:99 mm × 232 mm) observed in ultraviolet light and images (25 mm × 52 mm) acquired at the surface area and at mid-height of the specimen shown after segmentation

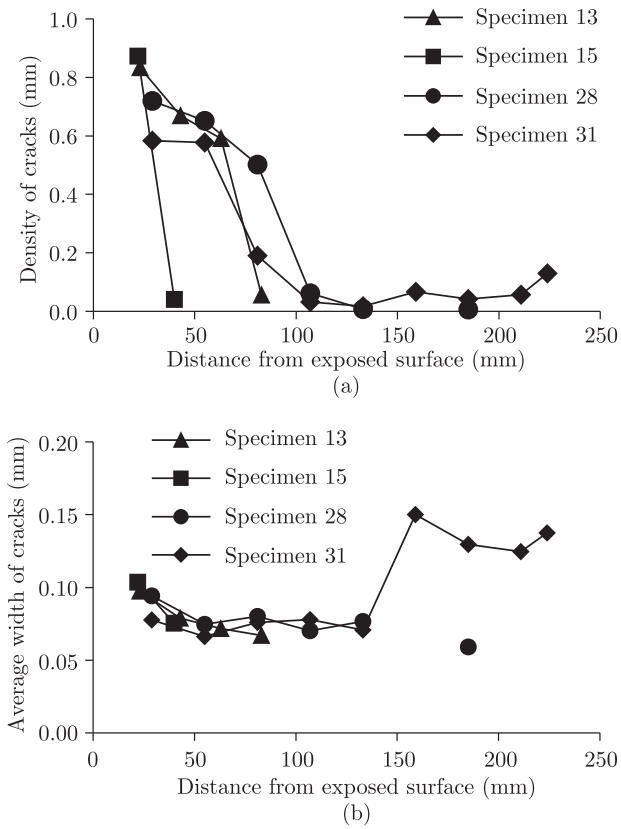

Fig. 15. Results of crack analysis: (a) density of cracks along the specimen height, (b) average width of cracks along the specimen height

Results of crack density analysis along the specimen height (at an increased distance from the external surface of the con-

Table 5
Results of crack analysis

Image	Dendritic length [mm]	Area [mm^2]	Average width [mm]	Density [mm/mm^2]	Areal fraction	Degree of orientation
F300_1	972.61	71.30	0.075	0.626	0.046	0.112
F300_2	516.42	38.65	0.073	0.332	0.025	0.152

crete element) permitted the determination of the extent of crack zone (Fig. 15a). Cracks were observed in low-temperature deteriorated concrete to a depth of 100 mm. The average width of cracks for each damaged concrete is similar (Fig. 15b). Only in specimen 31 were wider cracks below the concrete layer damaged by freezing at its early age observed. These cracks were introduced during the collapse of the structure.

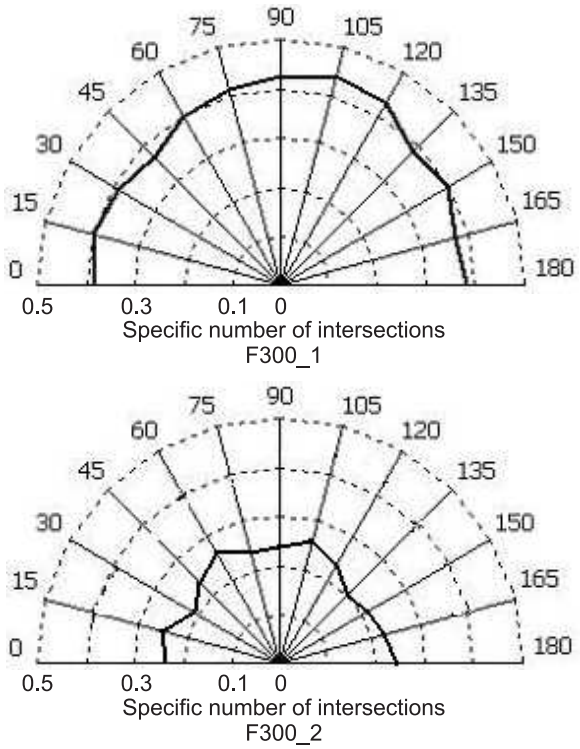

Fig. 16. Rose of the number of intersections for two images: F300_1 and F300_2

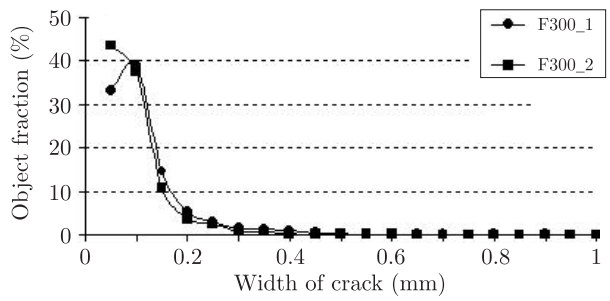

Fig. 17. Distribution of crack width on images F300_1 and F300_2

4.3. Concrete designed for tunnel walls. The crack system analysis was performed to evaluate concrete damage caused by freeze/thaw cycles. The tested specimen (150 mm cube) was taken from concrete prepared for a construction of a tunnel. The specimen was subjected to 300 freeze/thaw cycles. Two images (25 mm $\times$ 61 mm) were acquired in two areas of IRPS: first one – near the casting surface of the specimen (surface area), and second one – about 50 mm below (internal area).

Results showed that the crack density is almost two times higher in the surface area (Tabl.5). The average width of cracks is similar on two analysed images. By definition, degree of orientation ? takes the value 0 for a perfectly isotropic crack pattern and the value 1 when all the cracks have the same orientation. The determined degree of crack orientation and the roses of intercepts (Fig. 16) indicate random crack orientation.

Distribution of crack width is presented in Fig. 17 as a percentage object fraction in the range of crack widths from 0 mm to 1 mm. For the two images the distribution is similar, but only in the range of crack width to 0.1 mm; a higher percentage object fraction was obtained for image F300_2. In the range above 0.55 mm the percentage object fraction is equal to 0.

Observation and microscopic analysis indicate significant internal deterioration of the specimen. Results of crack analysis suggest the reduction of concrete resistance to penetration of aggressive agents from the environment and as a consequence a decrease its durability.

5. Conclusions

By means of optical fluorescent microscopy and an image analysis system a new method for identification and quantification of crack patterns in concrete was developed. Observation of the concrete surface in ultraviolet light using an optical microscope at the magnification of 10 times is sufficient to detect meso-level fine cracks and to provide automatic evaluation of the crack system. The proposed method provides a quantitative determination of the following crack system parameters: a dendritic length, an area, an average width, a density, an areal fraction, a degree of orientation and a distribution of crack widths.

The laboratory investigation revealed a good correlation between the density of cracks and the compressive strength, the depth of water penetration and the depth of chloride penetration determined on specimens intentionally subjected to damage due to freezing temperature during the hydration and hardening period. The compressive strength of concrete subjected to low-temperature action after mixing was significantly reduced in relation to the compressive strength of the reference concrete. The depth of water and chloride penetration in

concrete increased in damaged specimens by several times. In concretes exposed to –5°C the reduction of the compressive strength and the resistance to water and chloride penetration in concrete depends on the retardation of the initial freezing age of the concrete mixes.

The testing method was applied for concrete diagnostics on cores taken from several structures (industrial floor, parking slab) damaged by various mechanisms (mechanical, physical). Quantitative determination of the crack system provided data aiding the in-depth diagnosis of concrete quality in structural elements. The new test method has been found to be a valuable supplement to common concrete diagnostic methods.

REFERENCES

[1] R. François and G. Arliguie, "Effect of microcracking and cracking on the development of corrosion in reinforced concrete members", *Magazine of Concrete Research* 51, 143–150 (1999).

[2] C.M. Aldea, S.P. Shah, and A. Karr, "Permeability of cracked concrete", *Materials and Structures* 32, 370–376 (1999).

[3] Z. Li and S.P. Shah, "Localization of microcracking in concrete under uniaxial tension", *ACI Materials Journal* 91 (4), 372–381 (1994).

[4] J.P. Ollivier, "A non destructive procedure to observe the microcracks of concrete by scanning electron microscopy", *Cement and Concrete Research* 15 (6), 1055–1060 (1985).

[5] M.A. Glinicki and A. Litorowicz, "Application of UV image analysis for evaluation of thermal cracking in concrete", *Brittle Matrix Composites* 7, 101–109 (2003).

[6] F. O. Slate and S. Olsefski, "X-rays for study of internal structure and microcracking of concrete", *Journal of the American Concrete Institute* 60 (5), 575–587 (1963).

[7] A. Ammouche, J. Riss, D. Breysse, and J. Marchand, "Image analysis for the automated study of microcracks in concrete", *Cement and Concrete Composites, Special Issue: Image Analysis* 23, 267–278 (2001).

[8] P. Soroushian, M. Elzafraney, and A. Nossoni, "Specimen preparation and image processing and analysis technique for automated quantification of concrete microcracks and voids", *Cement and Concrete Research* 33, 1949–1962 (2003).

[9] E. Ringot and A. Bascoul, "About the analysis of microcracking in concrete", *Cement and Concrete Composites* 23, 261–266 (2001).

[10] A. Henrichsen and P. Laugesen, "Monitoring of concrete quality in high performance civil engineering constructions", *MRS Symposium Proc.* 370, 49–56 (1995).

[11] A. Litorowicz, "Influence of crack system quantified by means of optical fluorescent microscopy and image analysis on concrete properties", *Proc. 10th Euroseminar on Microscopy Applied to Building Materials*, Paisley, on CD (2005).

[12] NT Build 492, Concrete, *Mortar and Cement-Based Repair Materials: Chloride Migration Coefficient from Non-Steady-State Migration Experiments*, 1999.

[13] C.C. Yang, S.W. Cho, and R. Huang, "The relationship between charge passed and the chloride-ion concentration in concrete using steady-state chloride migration test", *Cement and Concrete Research* 32 (2), 217–222 (2002).

[14] K. Wang, S.P. Shah, and P. Phuaksuk, "Plastic shrinkage cracking in concrete materials - influence of fly ash and fibers", *ACI Materials Journal* 98 (6), 458–464 (2001).

[15] A.M. Brandt and M.A. Glinicki, "Concrete quality evaluation in a building that collapsed due to freezing of fresh concrete", *Conference on Construction Failures*, Międzyzdroje, (2005), (in Polish).